

doi.org/10.2217/rme.14.77

## **Repair of osteochondral defects in the minipig model by OPF hydrogel loaded with adipose-derived mesenchymal stem cells**

de Girolamo L<sup>1</sup>, Niada S<sup>1,2</sup>, Arrigoni E<sup>2</sup>, Di Giancamillo A<sup>1,3</sup>, Domeneghini C<sup>3</sup>, Dadsetan M<sup>4</sup>, Yaszemski MJ<sup>4</sup>, Gastaldi D<sup>5</sup>, Vena P<sup>5</sup>, Taffetani M<sup>5</sup>, Zerbi A<sup>1</sup>, Sansone V<sup>1,6</sup>, Peretti GM<sup>1,6</sup>, Brini AT<sup>1,2</sup>

<sup>1</sup>IRCCS Galeazzi Orthopaedic Institute, Milan, Italy

<sup>2</sup>Department of Biomedical, Surgical and Dental Sciences, University of Milan, Milan, Italy

<sup>3</sup>Department of Health, Animal Science and Food Safety, University of Milan, Milan, Italy

<sup>4</sup>Department of Orthopaedic Surgery, Mayo Clinic, College Of Medicine, Rochester, MN, USA

<sup>5</sup>LaBS-Laboratory of Biological Structure Mechanics, Department of Chemistry, Materials and Chemical Engineering Giulio Natta, Politecnico di Milano, Milan, Italy

<sup>6</sup>Department for Biomedical Sciences for Health, University of Milan, Milan, Italy

### **Corresponding Author:**

*Laura de Girolamo*

*IRCCS Istituto Ortopedico Galeazzi*

*Via R. Galeazzi 4, 20161 Milano, Italy*

*+39 02 66214059*

*[laura.degirolamo@grupposandonato.it](mailto:laura.degirolamo@grupposandonato.it)*

## ABSTRACT

**Aims:** Critical knee osteochondral defects in seven adult minipigs were treated with oligo(polyethylene glycol)fumarate (OPF) hydrogel combined with autologous or human adipose-derived stem cells (ASCs), and evaluated after 6 months. **Methods:** Four defects were made on the peripheral part of right trochleas (n=28), and treated with OPF scaffold alone or pre-seeded with ASCs. **Results:** A better-quality cartilage tissue characterized by improved biomechanical properties and higher collagen type II expression was observed in the defects treated by autologous or human ASC-loaded OPF; similarly this approach induced the regeneration of more mature bone with upregulation of collagen type I expression. **Conclusion:** This study provides the evidence that both porcine and human adipose-derived stem cells associated to OPF hydrogel allow improving osteochondral defect regeneration in a minipig model. **Keywords:** osteochondral defects, adipose-derived stem cells (ASCs), oligo(polyethylene glycol)fumarate hydrogel, bone, cartilage

## INTRODUCTION

The treatment of osteochondral defects represents one of the major and most problematic issues in the orthopaedic practice. One of the main obstacles arises from the disparity concerning both anatomy, composition and, most importantly, rate of healing of the articular cartilage (AC) and of the subchondral bone. Despite these two tissues exhibit considerably different structural composition, they constitute a single unit which acts as a whole in carrying its physiological function of absorbing mechanical stress for a suitable transmission of forces in the joints [1,2]. Furthermore, synergy between subchondral bone and AC is required for a mutual remodelling process [3]. One strategy to treat the entire osteochondral unit is the autologous or allogeneic transplantation, even though this approach presents some complications such as uneven surface, dislocation, donor site morbidity or lack of cadaveric graft [4,5]. To overcome these problems the employment of scaffolds could represent a valid alternative. Indeed, biomaterials could be differently moulded to fill properly osteochondral defect shapes and donor site morbidity is completely avoided. In the recent years different types of cells combined with a variety of supports have been tested in many tissue engineering preclinical studies. Beside autologous chondrocytes [6,7], mesenchymal stem cells (MSCs) are an attractive alternative for the treatment of osteochondral defects. MSCs were first isolated from bone marrow [8] and, the search for MSC-like cells in specific tissues and organs has led to the discovery of a variety of progenitor cells from several adult tissues [9-11] with multi-differentiation ability toward cells of

mesodermal origin, such as osteoblast- as well as chondrocytes-like cells [9]. Moreover, it has been shown in several pre-clinical studies, that these cells display the potential to restore and/or regenerate damaged tissues [12-14]. In particular, a great interest has been focused on cell-based therapies involving adipose-derived stem cells (ASCs). ASCs can be easily extracted with mild donor site morbidity or patient discomfort , and they showed a more potent immunomodulatory effect compared to bone marrow-derived stem cells (BMSCs), by the secretion of higher levels of factors, such as IL-6 and TGF- $\beta$ 1 [15]. Indeed, the low immunogenicity of ASCs has been exploited in several studies of allogeneic transplantation, shown to be safe and without adverse reactions such as inflammation and rejection [16,17].

Concerning the regenerative treatments for osteochondral defects, biphasic scaffolds able to support the growth of cartilage and bone have been developed [18-21]. However, since the microenvironment at the injured site acts by itself as a stimulus for the regeneration, the combined use of monophasic scaffolds and progenitor cells has been demonstrated to be efficient [22,23].

In this study, critical knee osteochondral defects were treated with bioconstructs made of a hydrogel of oligo (polyethylene glycol) fumarate (OPF) combined with either autologous, allogeneic or human ASCs in Yucatan miniature swine model and evaluated at 6 months of follow up, with the aim of proving the efficacy of ASCs combined with a resorbable soft material.

## **MATERIALS AND METHODS**

This research was partially funded by the Italian Ministry of Health.

### ***Scaffold preparation***

Oligo(polyethylene glycol) fumarate (OPF) was synthesized using polyethylene glycol (PEG) with the initial molecular weight of 10,000 as previously described [24]. Porous negatively charged hydrogels were made by dissolving 1 g OPF macromer and 0.1 g sodium methacrylate (SMA) in 2 ml deionized water containing 0.15% (w/w) Irgacure 2959 (Ciba-Specialty Chemicals, Tarrytown, NY, USA) and 300  $\mu$ l N-vinyl pyrrolidinone. In order to obtain hydrogels with 75% porosity, the resulting solution was mixed with sodium chloride (particle size, 300  $\mu$ m) at a ratio of 1:3 (W/W), and polymerized using 365 nm UV light at the intensity of  $\sim$ 8 mW/cm<sup>2</sup> (Black-Ray Model 100AP, Upland, CA, USA) for 30 min. Cylindrical hydrogel scaffolds (9 mm diameter, 8 mm height) were cut using a cork borer and placed in deionized water for 48h with 4-5 changes.

### ***ASC isolation, expansion and characterization***

Seven adult (12 months old) male Yucatan minipigs, with an average weight of  $73.5 \pm 2.2$  kg (range 71-77 kg), were included in the study. Animal care and surgery were approved by the Ethical and Technical Committee of the Italian Ministry of Health (CRABCC-22-2011); all the animal experiments were performed in accordance with both policies and principles of laboratory animal care and with the European Union guidelines (86/609/EEC) approved by the Italian Ministry of Health (Law 116/92), which was effective at the time of authorization.

During the first surgical procedure, upon shaving and disinfection, adipose tissue (~ 8 g) was harvested from the interscapular region of all animals. General anaesthesia was induced by intramuscular injection of a combination of ketamine (10mg/kg) and midazolam (0.5mg/kg) and maintained via inhalation of a mixture of isoflurane 4% in oxygen. The small incision was then sutured and the animals were administered once with tramadol (1mg/kg) and meloxicam (0.4 mg/kg) to control pain.

Minipig ASCs (mpASCs) were isolated from fat tissue after 0.1% type I collagenase digestion, as previously described [25], and then purified by adhesion culturing them in DMEM supplemented with 10% fetal bovine serum, 50 U/ml Penicillin, 50 µg/ml Streptomycin, and 2mM L-glutamine (Sigma–Aldrich, Milan, Italy) at 37° C in a humidified atmosphere with 5% CO<sub>2</sub>. At 80–90% of confluence, adherent cells were detached from the culture plates by incubation with trypsin/EDTA (0.5% trypsin/0.2% EDTA; Sigma–Aldrich) for 3 min at 37°C. Cells were plated at a density of  $5 \times 10^3$  cells/cm<sup>2</sup> for further expansion.

Human ASCs (huASCs) were isolated from waste adipose tissue from aesthetic liposuction of a female donor (age 61, BMI < 30 kg/m<sup>2</sup>, no metabolic disease) after informed consent and Institutional Review Board approval (M-SPER-014.ver7 for use of surgical waste) of Galeazzi Orthopaedic Institute, Milano, Italy, as previously described [26]. Human cells were produced as porcine ASCs, with the exception of the collagenase digestion (0.075%) and plating density ( $10^4$  cells/cm<sup>2</sup>).

Colony forming unit–fibroblast assay (CFU-F) was performed by plating in 6-well plates 1000 ASCs/well serial diluted [25,26].

For *in vitro* assessment, at passage 4, both mpASCs and huASCs were induced to differentiate towards cells of the osteogenic and chondrogenic lineages in specific culture conditions [25,27]. Osteogenic differentiation was assessed after 14 days evaluating alkaline phosphatase activity, collagen deposition by Sirius Red staining and calcified extracellular matrix deposition by Alizarin Red S staining, as previously described [28].

Chondrogenic differentiation was determined quantifying the sulfated glycosaminoglycans (GAGs) content according to the dimethylmethylene blue (DMMB) modified assay [27].

### ***Experimental design and surgical procedure***

About three weeks after fat tissue withdrawal,  $3 \times 10^6$  of undifferentiated either minipig or human ASCs, were seeded on each OPF cylindrical scaffold and let adhere overnight. Cell-free scaffolds followed identical procedure. Next day, the minipigs were surgically treated under general anaesthesia. With the animals in dorsal recumbence, a medial parapatellar incision and arthrotomy were performed on the right hind leg to expose the anterior aspect of the distal femur. Using a standardized core punch, four osteochondral lesions (9 mm in diameter, 8 mm in depth each) per knee were created in the trochlea periphery (Figure 1). The 28 defects were differently treated as reported in Table 1. Untreated defects were considered the negative controls (UNT group, n=7). Each scaffold was maintained into the lesion by press-fit.

After implantation, the joint capsule was closed and the wound was sutured in layers with bioabsorbable stitches. After surgery, the minipigs were treated at first with enrofloxacin (2 mg/kg IV) and amoxicillin (15mg/kg IM); then, with enrofloxacin (5 mg/kg die for 5 days IM) and meloxicam (0,4 mg/kg die for three days) to control pain. The animals were progressively allowed to free movements and carefully monitored until full recovery. Six months later, all animals were euthanized by IV injection of pentothal sodium (50 mg/kg) and potassium chloride (20 mg/kg); the right hind legs were explanted and then analysed by magnetic resonance imaging (MRI). Then, the joints were dissected, the treated portions retrieved en bloc and cut into four pieces corresponding to the four osteochondral defects, to allow independent analyses of each defect. Each single defect was prepared for further analyses. The contralateral legs were also explanted and used as controls.

### ***Macroscopic analysis***

Macroscopic signs of infection, inflammation, hypertrophy of the synovial membrane and tissue adhesions were assessed. The gross chondral surface was evaluated, taking into account the neo-formed tissue and the interface implant-host tissue. Signs of incomplete filling, matrix degradation, fusion between the different osteochondral defects and other possible features were recorded.

### ***MRI protocol***

The right hind limb of all animals and one control left limb were imaged by MRI. Examinations were performed using two 1,5 T magnetic field super conducting MR Systems (Avanto, Siemens Medical Solution,

Erlangen, Germany, gradient strength 45 mT/m, slew rate 200 T/m/ms, with a dedicated 8-channel knee coil, Invivo, Gainesville, FL, USA).

The hind limbs of minipigs were positioned with the knee extended and with the joint space in the middle of the coil. Lesions were studied with the following sequences:

- PD-TSE FS SPACE sequence on sagittal plane (Repetition Time [RT]/Echo Time [ET]: 1200/35; Field of View [FOV]: 170x170 mm; Matrix: 320x320; Slice Thickness: 1 mm; Voxel Size: 0.5x0.5x1 mm; Number of Slice: 60; scan time: 9 min, 2 sec)
- T2-weighted TSE sequence on sagittal plane (RT/TE: 3300/83; Flip angle: 150°; FOV: 180x180 mm; Matrix: 320x320; Slice Thickness: 3 mm; Voxel Size: 0.6x0.6x3 mm; number of slice: 20; scan time: 4 min, 1 sec)
- T1-weighted Vibe Water Excitation (WE) GE sequence on sagittal plane (RT/TE: 15.6/6.65; Flip angle: 12°; FOV: 200x160 mm; Matrix: 256x256; Slice Thickness: 1 mm; Voxel Size: 0.8x0.8x1 mm; number of slice: 72; scan time: 5 min, 45 sec)
- T1-weighted sequence on sagittal plane (RT/TE: 560/10; Flip angle: 143°; FOV: 160x160 mm; Matrix: 384x310; Slice Thickness: 2.5 mm; Voxel Size: 0.5x0.4x2.5 mm; number of slice: 20; scan time: 5 min, 14 sec)

Post-processing was performed on a dedicated workstation (Leonardo, Siemens Medical Solution, Forchheim, Germany). Images evaluations were performed by two experienced senior musculoskeletal radiologists.

MRI data were analysed by the modified 2D MOCART score [29,30] for the evaluation of *ex vivo* osteochondral samples, as reported in Table 2. The scale ranged between 0 and 100, where 0 was the worst and 100 the best scoring.

### ***Histological and immunohistochemical analysis***

The samples were dissected free of soft tissue, fixed in 10% buffered formalin for 24 hours at room temperature, and then decalcified in a formic acid-sodium citrate solution as described elsewhere [13]. After decalcification, samples were rinsed for 10 min in running water, and processed for paraffin embedding through a graded ethanol series. Four micrometer-thick sections were obtained and stained with Safranin-O following a standard protocol, for the evaluation of the structural details and GAGs deposition. Following rehydration, sections for immunohistochemical analyses were incubated in an aqueous solution of 1% H<sub>2</sub>O<sub>2</sub> for 30 min at room temperature, washed 3 times in PBS and then incubated overnight with either mouse anti-

collagen type I antibody or anti-collagen type II (both Chondrex Inc, Redmond, WA, USA; 1:500). Antigen retrieval was performed by treating the sections in citrate buffer, pH 6.0, in a microwave oven (2 times for 5 min at 500 W) for anti-collagen type I and with 2% hyaluronidase solution (Sigma-Aldrich) at room temperature for 30 min for anti-collagen type II. Antigen–antibody complexes were detected with a peroxidase-conjugated polymer, which carries secondary antibody molecules directed against mouse immunoglobulins (EnVision™+, DakoCytomation, Milan, Italy) applied for 60 min at room temperature. Peroxidase activity was detected with diaminobenzidine (DAB, DakoCytomation) as the substrate. For all the immunohistochemical procedures the samples were weakly counterstained with Mayer's hematoxylin, dehydrated, and permanently mounted. The specificity of anti-collagen type I or type II antibody was also assessed. Photomicrographs were taken with an Olympus BX51 microscope (Olympus, Milan, Italy) equipped with a digital camera and final magnifications were calculated. The sections were also analyzed with a polarized light microscope (Leica DM LP microscope, Leica Microsystems, Wetzlar, Germany) in order to investigate the tissue organization, referring to collagen fibers of the newly formed structures.

### ***Histological scoring***

Oriented histological specimens and stained with Safranin-O were evaluated to assess the quality of tissue repair [31]. The ICRS II scoring system was chosen [32]. It contains 14 parameters: an overall assessment and 13 parameters relating to both chondrocyte and tissue features (Table 3). Each parameter was scored using a 100 mm VAS (Visual Analog Scale), where 0 was considered as poor quality and 100 as very good quality. Three experienced blind researchers independently evaluated several sections of the all specimens for each group of treatment.

### ***Biomechanical test by nanoindentation***

The experiments were performed using a NanoTest Indenter (Micro-Materials Ltd., Wrexham, UK) equipped with a liquid cell to keep samples in a hydrated and fully saturated state. The sample preparation protocol was the following: i) each sample was thawed in a thermal bath at 37 °C for 45 min; ii) the samples were glued on a cylindrical aluminum stub equipped with a glass chamber and placed into the nanoindenter; iii) the chamber was filled with physiological solution (0.90% w/v of NaCl) and maintained to achieve the thermal and swelling equilibrium before running the tests.

Nanoindentation tests were carried out following a multiloading schedule in load control mode. The maximum load was applied by a series of load steps of increment 0.1 mN with a holding time of 120 sec at the end of

each load level. The maximum indentation force was ranging between 0.3 mN and 1 mN according to the sample compliance. The loading and unloading rates were 1 mN/sec and the tests were carried out with two spherical tips of radii  $R_{25}=25 \mu\text{m}$  and  $R_{400}=400 \mu\text{m}$ , respectively. The indentation modulus was computed according to the Hertzian theory for spherical indentation [33,34] by fitting the force-penetration data achieved at equilibrium. Table 4 reports the details of the indentation tests.

Tissue permeability was identified by suitably adapting the analytical solution available for the vertical displacement of the top surface of a poroelastic layer subjected to load-controlled confined compression test proposed by Biot [35]. The analytical solution was used to fit the force-displacement data  $h^j(\tau)$  collected during the spherical indentation, being  $j$  the load level. To this purpose, a dimensionless time  $\tau^j$  has been

introduced by following Oyen et al. [36] as  $\tau^j = \frac{P_2^j t}{\beta R h^j(t)}$  where  $\beta$  is a parameter identified through numerical

simulations and  $P_2^j$  plays the role of a diffusivity. Then, a two-parameters ( $P_1^j$  and  $P_2^j$ ) function is used to

best fit the creep curves [37]:  $h^j(\tau) = h^j(0) + P_1^j [g(\tau^j)]$  where  $h^j(0)$  is the indentation depth reached at the

beginning of each holding phase and  $g(\tau) = 1 - \sum_{m=0}^{\infty} \frac{8}{(1+2m)^4 \pi^4 \tau_R} \left[ e^{-(1+2m)^2 \pi^2 (\tau - \tau_R)} - e^{-(1+2m)^2 \pi^2 \tau} \right]$ . Finally,

permeability is obtained, for each load level  $j$ , as  $k^j = \frac{P_2^j}{M_{eq}}$ .

### **Statistical analysis**

Data are expressed as mean  $\pm$  standard deviation (SD) and statistical analysis was performed using Student's t-test, unless indicated otherwise. For the histological scoring analysis of variance stratified for each item was used. Data were analyzed using GraphPad Prism v5.00 (GraphPad Software, San Diego, CA). In all cases  $p < 0.05$  was considered statistically significant.

## **RESULTS**

### ***Both mpASCs and huASCs efficiently differentiate into osteogenic and chondrogenic lineages in vitro***

mpASCs were isolated from 7 minipigs with an average yield of  $5.6 \times 10^4 \pm 1.4 \times 10^4$  cells/ml of raw adipose tissue, quite comparable to that obtained from the human fat tissue used in this study ( $8.5 \times 10^4$  cells/ml) (Figure 2A). ASCs isolated from minipigs are smaller and with a more round shape when compared to human ASCs (Figure 2B), as we also previously described [25]. One week later, all the populations, started rapidly to grow with variable proliferation rates, as shown in figure 2C. From passage 2 to 4 the average doubling time was  $60.3 \pm 16.5$  hours (range 46.9–112.3 hours) for the minipig cells, and it appears longer for the human ones ( $101.9 \pm 22.8$  hours). mpASC clonogenic ability ( $16.1 \pm 7.2\%$ ) was assessed between



passage 2 and 4, and it was more pronounced than that determined for huASCs ( $10.1 \pm 1.4\%$ , see Figure 2A). To test their multi-differentiation potential *in vitro*, mpASCs and huASCs were induced by osteogenic and chondrogenic stimuli, and in suitable culture conditions for 2 and 3 weeks, respectively. *In vitro* osteo-differentiated ASCs significantly increased the osteogenic markers with respect to the control cells, such as alkaline phosphatase (Figure 3A), calcified extracellular matrix (Figure 3B) and collagen (Figure 3C) deposition of about 440%, 151%, and 110%, respectively for mpASCs, and of about 104%, 152% and 401% respectively for human cells. In addition, chondro-differentiated mpASCs and huASCs, grown in pellet culture for 21 days, increased the amount of GAGs compared to undifferentiated cells (92% and 28%, respectively) (Figure 3D).

#### ***Minipigs well tolerated the surgical procedures and the bio-implants***

After a short period of limping, lasting not more than 14 days from surgery, all the minipigs recovered a normal gait, without any functional limitations. Knee swelling was present in all the animals for about 3 weeks post-surgery.

#### ***OPF alone or in combination with ASCs improved MOCART scores***

Magnetic resonance of all treated joints was performed immediately after the explant of the limbs, before the arthrotomy. As revealed by the modified 2D MOCART scale, MR confirmed the appropriateness of our severe critical defect model, as the untreated group reached only 25% of the repair rate, while the benefit of the use of both seeded and unseeded scaffolds was detectable. Indeed, all the scaffold-treated defects showed significantly higher scores in comparison to the untreated ones (Figure 4), with no differences among the OPF and OPF-ASC groups. Indeed, from a qualitative point of view, a mild scaffold resorption was observed in the scaffold groups: the defects were partially invaded by bone-like tissue, with some irregularities of the superficial layer. No bone absorption as well as no signs of edema were seen around the scaffold.

A good integration of the scaffold to the bone was observed, with no signs of reaction in the bone tissue around the implanted scaffold. Empty defects showed incomplete fibrous tissue filling, reaching no more than 2/3 of the original defect, covered by fibrotic tissue of low signal.

Following arthrotomy, joint inspection did not reveal any sign of inflammation, as well as adhesion, hypertrophy or fibrosis of synovial membrane. The surface of all defects showed small cylindrical lacks of substance, sometimes associated with signs of vascular infiltration (Figure 5, A2-A5).

In only one animal signs of local infection were observed and it was excluded from the study to assure the reliability of the results. Out of the four defects of this minipig, two had been treated with allogeneic cells, one with OPF alone and one left empty. In this study the arranged defects to be treated with allogeneic cells were three in total (Table 1); for this reason, even though no macroscopical and histological differences between the only retrieved OPF-Allo construct and the ones produced with autologous cells were observed, the data about this group are not shown and no statistical analysis was performed.

***ASCs seeded on OPF allowed the regeneration of more mature bone and the upregulation of collagen type II expression at cartilage level***

In both unseeded and mp-ASC or hu-ASC seeded scaffolds most of the tissue present into the defects was fibrocartilage, mainly located in the central part of the defects (Figure 5, B3-B5). In general, they were less intensely Safranin-O positive respect to the native articular cartilage (Figure 5, B1), showing a lower content of glycosaminoglycans. Cartilage was present only at the edge of the defects in all the scaffold-treated groups (Figure 5, B3-B5). In terms of subchondral bone repair, a bone formation process was evident, with osteoblasts lining the surfaces of the construct, above all in OPF-A and OPF-Hu groups (Figure 5, C3-C5). Interestingly, more mature bone, with the presence of bone lamellas, was observed in OPF-Hu treated defects.

In the untreated defects, the repair tissue was characterized by a strong depletion of glycosaminoglycan content, as shown by the poorly intense Safranin-O staining; overall, it was constituted mainly by fibrous tissue, with blood vessels and a disorganized extracellular matrix, protruding into the defect cavity (cartilage-like tissue flow). Fibrocartilage was very scarcely represented (Figure 5, B2), and restoration of the subchondral bone was insufficient and very immature as it started with endochondral bone formation at the borders of the defect (Figure 5, C2).

Anyway, cartilage hypertrophy was not observed in any sample of the experimental groups.

As shown in the healthy joint (Fig. 5, D1), analysis by polarized light microscopy allowed to evaluate the presence of the collagen components, of primary and secondary bone, the differentiation between mature and developing osteons, and the bone lamellas and their orientation. In the untreated group, collagen fibrils were not organized in lamellar form (Figure 5, D2), whereas in both seeded and unseeded OPF defects, an organized distribution of collagen fibrils was observed. In particular, the deposition of lamellar bone occurred

within the pores of the scaffolds (Figure 5, D3-D5), without any relevant differences among unseeded and mp-ASC or hu-ASC seeded scaffolds.

In the defects treated with both OPF-A and OPF-Hu a considerable quantity of collagen type II was present (Figure 5, E4-E5), and it was comparable to the one of the healthy cartilage (Figure 5, E1). In contrast, the collagen II immunostaining was much less evident in both untreated and unseeded OPF groups (Figure 5, E2-E3). However, in all the groups, the inner part of the neo-cartilage of the repaired tissue contained scarce collagen II immunostaining positive tissue (data not shown). In addition, the neo-formed bone was more positive for collagen type I in OPF-A and OPF-Hu groups in comparison to untreated and unseeded OPF groups (Figure 5, F2-F5).

According to ICRS II scores, significant differences were found between OPF and OPF-A groups for some parameters. In particular, tidemark formation, vascularization, matrix staining, cell morphology and tissue morphology scored significantly higher in the group treated with OPF-A with respect to OPF ( $p < 0.05$ ). Just surface assessment score was significantly lower in OPF-A compared to OPF. No other differences were found between the two scaffold groups. However, untreated group showed significantly higher scores for some parameters, including formation of tidemark, subchondral abnormalities and basal integration, as well as parameters concerning the surface assessment, suggesting that the presence of residual scaffold at the defect site negatively affected this kind of evaluations (Figure 6).

#### ***Neo-cartilage of OPF-A group showed biomechanical properties similar to the native tissue ones***

The indentation modulus at equilibrium  $M_{eq}$ , standard deviation identified for healthy control, OPF-A, OPF and untreated samples are reported in Figure 7 for both the 25  $\mu\text{m}$  (A) and 400  $\mu\text{m}$  (B) tips.

$R^2$  fitting parameter was found in the following ranges. For the data ( $F_L - h_{eq}$ ) measured using the 25  $\mu\text{m}$  tip: [0.97 - 0.98], healthy cartilage and OPF-A samples; [0.92 - 0.93], OPF samples; [0.86 - 0.88], untreated samples. For the data ( $F_L - h_{eq}$ ) measured using the 400  $\mu\text{m}$  tip: [0.97 - 0.98], healthy cartilage and OPF-A samples; [0.89 - 0.91], OPF samples; [0.86 - 0.87], untreated samples.

In all cases, indentation moduli measured using the small tip radius is larger than those found with the large tip radius. Healthy cartilage exhibits an indentation modulus ( $603 \pm 199$  kPa) similar than that found for OPF-A samples ( $545 \pm 96$  kPa) with  $R_{25}$  tip. A similar consideration holds for the large tip radius: healthy cartilage and OPF-A samples exhibited an indentation modulus of  $238 \text{ kPa} \pm 68 \text{ kPa}$  and  $272 \pm 29$  kPa, respectively. Both OPF and untreated samples showed an indentation modulus at equilibrium significantly smaller than that

found for healthy cartilage and OPF-A samples. In particular,  $M_{eq}$  for OPF sample was  $268 \pm 102$  kPa and  $110 \pm 10$  kPa for  $R_{25}$  and  $R_{400}$ , respectively (both  $p < 0.05$  with respect to native cartilage and OPF-A group);  $M_{eq}$  for untreated sample was  $292 \pm 47$  kPa and  $81 \pm 25$  kPa for  $R_{25}$  and  $R_{400}$ , respectively (both  $p < 0.05$  with respect to native cartilage and OPF-A group). No appreciable difference was found between OPF and untreated samples (Figure 7).

The tissue permeability  $k$  is identified for both indenter tips and for each load level. The  $k$  parameter was calculated for healthy and OPF-A samples only for which the creep response was fitted with  $R^2$  values greater than 0.8. The OPF and untreated samples exhibited creep curves which were fitted with  $R^2$  values lower than 0.7, therefore the poroelastic fitting model was considered unsuited.

Averaged values of the tissue permeability over all the load levels are:  $2.05 \pm 1.10 \times 10^{-15}$  for  $R_{400}$  and  $9.08 \pm 0.68 \times 10^{-17}$  for  $R_{25}$  in case of healthy cartilage sample;  $1.56 \pm 0.45 \times 10^{-15}$  for  $R_{400}$  and  $1.38 \pm 1.11 \times 10^{-16}$  for  $R_{25}$  in case of OPF-A sample. In Figure 8 the decreasing trend of permeability is instead presented for both the samples (mean values are shown) with respect to the equivalent deformation, computed as the ratio between the current contact length and the indenter radius. Engineered construct appeared slightly less permeable at smaller deformation.

In Figure 9 normalized creep displacement  $h$  - ranging from 0 (instantaneous) to 1 (long term) - vs natural time and normalized time [36] are reported. Only selected curves are presented for the healthy cartilage (Figure 9A), OPF-A (Figure 9B) and OPF (Figure 9C) samples for both the two tips. A complete overlap between creep curves vs normalized time collected at different loads and different tip radii is found for the healthy cartilage and for the OPF-A samples. This indicates that fluid flow through the porous matrix is the main dissipation mechanism; whereas, the creep response of OPF could not be fitted with the poroelastic fitting function so, no creep curves vs normalized time are available (Figure 9C).

## **DISCUSSION**

In the last two decades a wide variety of biological approaches have been proposed for the treatment of chondral and osteochondral defects, such as the use of multilayered scaffolds, enhanced or not by the use of progenitor cells or terminally differentiated chondrocytes, to provide a proper support to the different tissues [19-21,38]. Although these methods have shown promising results, they still have to be validated, and the development of an engineered graft before implantation to support an optimal repair needs further investigations. One of the main difficulties in selecting the most suitable approach is the great heterogeneity

among the studies, including different animal models which differ in body weight and joint characteristics (mouse [39], rat [40], rabbit [41], sheep [18,42], pigs [21,39]), several scaffolds and different cell populations [20]. Moreover, size of the lesions and the follow up duration are also parameters which differ considerably among studies [22,43].

OPF hydrogels have been previously well characterized and they have been shown to efficiently support bone regeneration [44]. A few reports concerning their use for osteochondral regeneration have been recently published. Hui et al showed usefulness of OPF hydrogel for cartilage regeneration in a swine model [43]; in another study, bone marrow-derived mesenchymal stem cells, in association with OPF hydrogel scaffold, were used with satisfactory results to treat chondral defect (6mm diameter, 1mm depth) in a porcine model [22]. In our study critical osteochondral defects were treated with a negatively charged SMA modified OPF hydrogel combined with either autologous or human ASCs in immunocompetent minipigs. Adult animals were chosen to reduce the spontaneous reparative process occurring in younger subjects and thus to obtain results more comparable to human adults. Our findings show that, six months after implantation, expanded undifferentiated ASCs seeded on OPF hydrogel were able to improve the biomechanical properties of the newly formed cartilage with respect to the defects treated with OPF alone. Indeed only the neo-cartilage found in the cell-loaded scaffold groups displayed poroelastic behavior, as well as indentation modulus comparable to native cartilage. In particular indentation modulus found for small tips is higher than that found with larger tips. This is consistent with previous published data and can be justified considering the microstructural architecture of the tissues which are loaded in different ways when applying different tip radii [45]. The permeability decrease with increasing strain is a well-known phenomenon, which can be easily justified by the change in porous architecture upon compression of the tissue. This creep response, i.e. the overlapping of the normalized displacement vs normalized time, is consistent with a poroelastic dissipation mechanism involved in the fluid flow through the porous matrix. On the other hand, the creep response of OPF and untreated samples could not fit with the poroelastic interpolation function. This indicates that other dissipation mechanisms are involved in these samples in addition to the fluid-flow through the porous matrix.

Furthermore, although histological observations indicated that cartilage regeneration was still in progress in all the samples, the use of ASCs associated with scaffolds allowed an improvement in collagen type II expression, matrix staining, tissue and cell morphology and formation of tidemark compared to scaffolds

alone. On the other hand, some parameters of ICRS II scale scored higher in the untreated lesions in comparison to the lesions treated with scaffolds, in particular those evaluating the surface quality. These data could be attributed to the lack of scaffold in this group that allowed the defects to be easily filled by tissue. Indeed, both radiological and histological analyses revealed that 6 months after implantation, scaffolds were still detected at the defect site. However, the untreated defects were fulfilled by fibrous unorganized tissue, characterized by very poor histological and biomechanical properties. Moreover, untreated defects showed a significantly lower signal intensity and worse scores in terms of adhesion and effusion when compared to the defects treated with scaffold, as demonstrated by 2D-MOCART score based on magnetic resonance images. Considering bone regeneration, in all the OPF+ASCs defects a more mature tissue characterized by a higher expression of collagen type I, compared to untreated or unseeded OPF groups, was observed. ASCs derived from several animal species, as well as from humans, have been shown to be able to differentiate into osteoblast-like cells *in-vitro* [25,26,46], as well as to promote bone regeneration in animal models [13,14]. This properties may be related to the ASC multi-differentiation potential and to their pro-angiogenic ability [47] through the secretion of factors such as VEGF, HGF and TGF- $\beta$  [48]. However, ASCs seemed to inhibit the vascularization process of newly formed cartilage, as evaluated by the ICRS II score. A possible explanation of this phenomenon could be that ASC can or cannot release angiogenic factors depending on the different cross-talk between them and the resident cells at the site of injury [49]. In our model, we used undifferentiated ASCs underwent to minimal manipulation in view of a possible easier way to translate this approach into the clinic. Moreover, this decision was also influenced by recent evidences on the mechanism of action of mesenchymal stem cells. Indeed, while at the beginning the attention was mainly focused on their ability to differentiate in specific cell lineages, more recently it was proposed that their therapeutic benefits are largely dependent on their ability to act as a drug store of trophic factors [50] and as modulators of immune response [51]. From this point of view, one of the main action of mesenchymal stem cells is also to support resident cells, which most likely are the major effectors of the described tissue replacement. Moreover, several soluble mediators, able to promote angiogenesis, tissue regeneration and remodeling, immune cell activation or suppression, and cellular recruitment, seems to be released according to the needs of the damaged environment [49]. For this reason we applied bioconstructs seeded with undifferentiated

cells, which are known to react to the most proper stimuli induced at the lesion site, and in particular we selected a monophasic scaffold without adding any other external stimuli, such as growth factors.

Undifferentiated MSCs express low levels of HLA (human leukocyte antigen) class I and II, that give them a so-called “stealth” ability not to be recognized as not self by the host immune system in allogeneic implants [52]. Despite this feature it has been shown that in some cases MSCs were able to elicit an immuneresponse in both animal studies and clinical trials [53,54]; on the other hand other studies support the feasibility and the effectiveness of the use of ASCs in allogeneic animal model [55,56].

In our study, no evident immune response have been detected; indeed all animals, monitored during the entire follow-up period, showed comparable clinical outcome independently from the use of either human or autologous cells, confirming the low immunogenicity of ASCs.

From the effectiveness point of view, the slight differences between human and animal-derived ASCs [25] might represent a limit when translating preclinical data into clinical application. In this study the effects elicited by autologous and human ASCs–based bioconstructs were compared in order to provide informations about the behavior of both these cell types at the site of injury. Indeed, one of the mostimportant criticism about their heterologous use is that cells could behave in a different way when they are in presence of xenostimuli (cytokines, growth factors, etc), since the cross-talk between implanted and resident cells might be slightly distorted. However, although the limited number of defects treated with human ASCs, our data show that both autologous and human OPF+ASCs constructs are able to ameliorate the subchondral bone and the newly formed cartilage properties if compared to the scaffold alone. Interestingly, the more mature bone, characterized by the presence of very mature bone lamellas, was observed indefects treated with human bio-construct.

One of the limitations of our study concerns the cell seeding on OPF scaffolds; indeed, due to the limited number of defects, a cell dose-response study was not performed, as a fixed number of cells was seeded in all the defects. Although ASCs were not labeled, the differences in term of new tissue quality found between seeded and unseeded hydrogels support the hypothesis of a direct cell involvement in the regeneration process, probably mainly by means of their paracrine effect.

## **CONCLUSIONS**

This study provides the evidence that both porcine and human adipose-derived stem cells associated to OPF hydrogel allow improving osteochondral defect regeneration. The swine model employed here

confirmed to be reliable for testing regenerative strategies for osteochondral repair. Our data confirms the suitability of OPF as biomaterial for bone regeneration, whereas it seems to be not particularly prone to guide a proper chondral regeneration. This scarce effectiveness can be partially reverted by the combination of ASCs with the hydrogel, as demonstrated by the improvement of the mechanical properties of the newly formed chondral tissue. Various parameters, including scaffold pore dimensions, possible association with growth factors, number of cells and biodynamic construct formation, need to be considered before planning any clinical application of this model.

## **FUTURE PERSPECTIVE**

Due to their availability and low-immunogenicity, ASCs represent an optimal mesenchymal cell type for regenerative purpose and their use has been already proposed for the treatment of different pathologies. However, the several concerns about their use still cause a gap between the pre-clinical studies and the clinical application. Studies in large animal model can help in filling this gap, as they can provide useful and reliable informations about the possible use of these cells in human. Our positive results allow to speculate the effectiveness of ASCs in combination with scaffolds also to repair severe osteochondral defects in patients with indications for this kind of treatment, although further confirmation needs to be achieved by specific clinical trials. Moreover, in the future to extend this treatment to the general population it is also necessary to pass through an economical sustainability process.

## **EXECUTIVE SUMMARY**

### **INTRODUCTION**

- The treatment of osteochondral defects represents one of the major and most problematic issues in the orthopaedic practice.
- The combined use of monophasic scaffolds and progenitor cells seems to be a promising approach.
- Adipose tissue is a smart source of mesenchymal stem cells characterized by good clonogenic ability, proliferation rate and multi-differentiation potential.

### **METHODS**

- Experimental osteochondral defects of minipigs' trochleas were treated with OPF scaffold alone or pre-seeded with both autologous and human ASCs. The outcome was evaluated after 6 months from surgery.

### **RESULTS**



- All the treatments based on the combination of both porcine and human ASCs and OPF hydrogel were safe and did not elicit any immune reaction.
- Both autologous and human ASCs seeded on OPF allow a better-quality cartilage tissue regeneration with respect to unseeded scaffold, with improved biomechanical properties and higher collagen type II expression. In all cases cartilage was not mature yet, probably because the regeneration process was slower than the expected since adult animals were used.
- Both autologous and human ASCs seeded on OPF allow the regeneration of more mature bone with upregulation of collagen type I expression.

## **DISCUSSION**

- Minipig represents an appropriate animal model to test tissue engineering-based treatments for severe osteochondral defects.
- This study supports the feasibility of the treatment of osteochondral defects with autologous or heterologous ASCs in association with OPF hydrogel, confirming the low immunogenicity of these cells.

## **ACKNOWLEDGEMENTS**

The Authors thanks Alessandro Addis, Marino Campagnol, Marco Pamovio and Marco Melato for their very valid work with animal care and help in surgery; Deborah Stanco and Silvia Molinari for their help in the *in vitro* experiments; Stefano Turolla, Simone Miliano and Sonia Denti for their contribution in MRI evaluations; Alessandro Nonis for the statistical support. This work has been partially supported by the Italian Ministry of Health.

## **DISCLOSURE**

None of the authors have any relevant affiliations or financial involvements to disclose.

## REFERENCES

1. Madry H, van Dijk CN, Mueller-Gerbl M. The basic science of the subchondral bone. *Knee Surg Sports Traumatol Arthrosc.* 18, 419-33 (2010).  
\*\*This review provides insights into the anatomy, morphology, and pathology of the subchondral bone; its deep knowledge is fundamental in the cartilage repair setting, as articular cartilage defects often arise from or extend into the subchondral bone.
2. Hoshino A, Wallace WA. Impact-absorbing properties of the human knee. *J Bone Joint Surg Br.* 69, 807-11 (1987).
3. Mahjoub M, Berenbaum F, Houard X. Why subchondral bone in osteoarthritis? The importance of the cartilage bone interface in osteoarthritis. *Osteoporos Int.* 23 Suppl 8, S841-6 (2012).
4. Madry H, Grun UW, Knutsen G. Cartilage repair and joint preservation: medical and surgical treatment options. *Dtsch Arztebl Int.* 108, 669-77 (2011).
5. Pape D, Filardo G, Kon E, van Dijk CN, Madry H. Disease-specific clinical problems associated with the subchondral bone. *Knee Surg Sports Traumatol Arthrosc.* 18, 448-62 (2010).
6. Foldager CB. Advances in autologous chondrocyte implantation and related techniques for cartilage repair. *Dan Med J.* 60, B4600 (2013).
7. Lee KT, Kim JS, Young KW *et al.* The use of fibrin matrix-mixed gel-type autologous chondrocyte implantation in the treatment for osteochondral lesions of the talus. *Knee Surg Sports Traumatol Arthrosc.* 21, 1251-60 (2013).
8. Pittenger MF, Mackay AM, Beck SC *et al.* Multilineage potential of adult human mesenchymal stem cells. *Science* 284, 143-7 (1999).
9. Zuk PA, Zhu M, Ashjian P *et al.* Human adipose tissue is a source of multipotent stem cells. *Mol Biol Cell.* 13, 4279-95 (2002).
10. Fukuchi Y, Nakajima H, Sugiyama D, Hirose I, Kitamura T, Tsuji K. Human placenta-derived cells have mesenchymal stem/progenitor cell potential. *Stem Cells.* 22, 649-58 (2004).
11. Lu LL, Liu YJ, Yang SG *et al.* Isolation and characterization of human umbilical cord mesenchymal stem cells with hematopoiesis-supportive function and other potentials. *Haematologica.* 91, 1017-26 (2006).
12. Qi Y, Zhao T, Xu K, Dai T, Yan W. The restoration of full-thickness cartilage defects with mesenchymal stem cells (MSCs) loaded and cross-linked bilayer collagen scaffolds on rabbit model. *Mol Biol Rep.* 39, 1231-7 (2012).
13. de Girolamo L, Arrigoni E, Stanco D *et al.* Role of autologous rabbit adipose-derived stem cells in the early phases of the repairing process of critical bone defects. *J Orthop Res.* 29, 100-8 (2011).  
\*This work highlights the usefulness of a cell-scaffold construct involving adipose-derived stem cells not pre-differentiated in vitro for critical-size bone defect repair in an animal model.
14. Park BH, Zhou L, Jang KY *et al.* Enhancement of tibial regeneration in a rat model by adipose-derived stromal cells in a PLGA scaffold. *Bone.* 51, 313-23 (2012).
15. Melief SM, Zwaginga JJ, Fibbe WE, Roelofs H. Adipose tissue-derived multipotent stromal cells have a higher immunomodulatory capacity than their bone marrow-derived counterparts. *Stem Cells Transl Med.* 2, 455-63 (2013).
16. Liu GB, Cheng YX, Feng YK *et al.* Adipose-derived stem cells promote peripheral nerve repair. *Arch Med Sci.* 7, 592-6 (2011).

17. Gutierrez-Fernandez M, Rodriguez-Frutos B, Ramos-Cejudo J *et al.* Effects of intravenous administration of allogenic bone marrow- and adipose tissue-derived mesenchymal stem cells on functional recovery and brain repair markers in experimental ischemic stroke. *Stem Cell Res Ther.* 4, 11 (2013).
18. Kon E, Delcogliano M, Filardo G *et al.* Orderly osteochondral regeneration in a sheep model using a novel nano-composite multilayered biomaterial. *J Orthop Res.* 28, 116-24 (2010).
19. Kim K, Lam J, Lu S *et al.* Osteochondral tissue regeneration using a bilayered composite hydrogel with modulating dual growth factor release kinetics in a rabbit model. *J Control Release.* 168, 166-78 (2013).
20. Martin I, Miot S, Barbero A, Jakob M, Wendt D. Osteochondral tissue engineering. *J Biomech.* 40, 750-65 (2007).
21. Schek RM, Taboas JM, Segvich SJ, Hollister SJ, Krebsbach PH. Engineered osteochondral grafts using biphasic composite solid free-form fabricated scaffolds. *Tissue Eng.* 10, 1376-85 (2004).
22. Lim CT, Ren X, Afizah MH *et al.* Repair of Osteochondral Defects with Rehydrated Freeze-Dried Oligo[Poly(Ethylene Glycol) Fumarate] Hydrogels Seeded with Bone Marrow Mesenchymal Stem Cells in a Porcine Model. *Tissue Eng Part A.* 19, 1852-61 (2013).
23. Nathan S, Das De S, Thambyah A, Fen C, Goh J, Lee EH. Cell-based therapy in the repair of osteochondral defects: a novel use for adipose tissue. *Tissue Eng.* 9, 733-44 (2003).
24. Jo S, Shin H, Mikos AG. Modification of oligo(poly(ethylene glycol) fumarate) macromer with a GRGD peptide for the preparation of functionalized polymer networks. *Biomacromolecules.* 2, 255-61 (2001).
25. Arrigoni E, Lopa S, de Girolamo L, Stanco D, Brini AT. Isolation, characterization and osteogenic differentiation of adipose-derived stem cells: from small to large animal models. *Cell Tissue Res.* 338, 401-11 (2009).
26. de Girolamo L, Lopa S, Arrigoni E, Sartori MF, Baruffaldi Preis FW, Brini AT. Human adipose-derived stem cells isolated from young and elderly women: their differentiation potential and scaffold interaction during in vitro osteoblastic differentiation. *Cytotherapy.* 11, 793-803 (2009).
27. de Girolamo L, Sartori MF, Arrigoni E *et al.* Human adipose-derived stem cells as future tools in tissue regeneration: osteogenic differentiation and cell-scaffold interaction. *Int J Artif Organs.* 31, 467-79 (2008).
28. Brini AT, Niada S, Lambertini E *et al.* Chondrogenic potential of human mesenchymal stem cells and expression of slug transcription factor. *J Tissue Eng Regen Med.* (2013).
29. Goebel L, Orth P, Muller A *et al.* Experimental scoring systems for macroscopic articular cartilage repair correlate with the MOCART score assessed by a high-field MRI at 9.4 T--comparative evaluation of five macroscopic scoring systems in a large animal cartilage defect model. *Osteoarthritis Cartilage.* 20, 1046-55 (2012).
30. Marlovits S, Singer P, Zeller P, Mandl I, Haller J, Trattnig S. Magnetic resonance observation of cartilage repair tissue (MOCART) for the evaluation of autologous chondrocyte transplantation: determination of interobserver variability and correlation to clinical outcome after 2 years. *Eur J Radiol.* 57, 16-23 (2006).
31. Hoemann CD, Chen G, Marchand C *et al.* Scaffold-guided subchondral bone repair: implication of neutrophils and alternatively activated arginase-1+ macrophages. *Am J Sports Med.* 38, 1845-56 (2010).

32. Mainil-Varlet P, Van Damme B, Nestic D, Knutsen G, Kandel R, Roberts S. A new histology scoring system for the assessment of the quality of human cartilage repair: ICRS II. *Am J Sports Med.* 38, 880-90 (2010).  
\*\*This work first describes a validated scoring system for the evaluation of the quality of repaired cartilage from biopsy specimens based on histological observation.
33. Johnson KL. Contact mechanics. *Cambridge University Press.* (1985).
34. Field JS, Swain MV. A simple predictive model for spherical indentation. *Journal of Materials Research.* 8, 297-306 (1993).
35. Biot MA. Theory of elasticity and consolidation for a porous anisotropic solid. *J Appl Phys.* 26, 182-185 (1955).  
\*\*This is a fundamental work which lays the basis for the analysis of the time dependent behavior of poroelastic anisotropic solids and it evaluates analytically the case of compression test.
36. Oyen M, Shean T, Strange D, Galli M. Size effect in indentation of hydrated biological tissues. *J Mater Res.* 27, 245-255 (2012)  
\*This is one of the first works in which the dependence of the mechanical properties of hydrated biological tissues on the characteristic lengths of the experiment is quantitatively assessed with specific reference to indentation tests.
37. Taffetani M, Gastaldi D, Gottardi R, Raiteri R, Vena P. Poroelastic response of articular cartilage by nanoindentation creep tests at different characteristic lengths. *Med Eng Phys.* 36, 850-8 (2014)
38. Duan P, Pan Z, Cao L *et al.* The effects of pore size in bilayered poly(lactide-co-glycolide) scaffolds on restoring osteochondral defects in rabbits. *J Biomed Mater Res A.* (2013).
39. Peretti GM, Xu JW, Bonassar LJ, Kirchoff CH, Yaremchuk MJ, Randolph MA. Review of injectable cartilage engineering using fibrin gel in mice and swine models. *Tissue Eng.* 12, 1151-68 (2006).
40. Gao J, Dennis JE, Solchaga LA, Awadallah AS, Goldberg VM, Caplan AI. Tissue-engineered fabrication of an osteochondral composite graft using rat bone marrow-derived mesenchymal stem cells. *Tissue Eng.* 7, 363-71 (2001).
41. Schaefer D, Martin I, Jundt G *et al.* Tissue-engineered composites for the repair of large osteochondral defects. *Arthritis Rheum.* 46, 2524-34 (2002).
42. Kandel RA, Grynepas M, Pilliar R *et al.* Repair of osteochondral defects with biphasic cartilage- calcium polyphosphate constructs in a sheep model. *Biomaterials.* 27, 4120-31 (2006).
43. Hui JH, Ren X, Afizah MH, Chian KS, Mikos AG. Oligo[poly(ethylene glycol)fumarate] hydrogel enhances osteochondral repair in porcine femoral condyle defects. *Clin Orthop Relat Res.* 471, 1174-85 (2013).  
\*This work describes the improvement of cartilage regeneration in a micropig model of cartilage defect using Oligo[poly(ethylene glycol)fumarate] hydrogel but also suggests the requirement of combining this scaffold with other "tissue-regenerating mediators" to ameliorate its regenerative capability.
44. Dadsetan M, Giuliani M, Wanivenhaus F, Brett Runge M, Charlesworth JE, Yaszemski MJ. Incorporation of phosphate group modulates bone cell attachment and differentiation on oligo(polyethylene glycol) fumarate hydrogel. *Acta Biomater.* 8, 1430-9 (2012).
45. Simha NK, Jin H, Hall ML, Chiravarambath S, Lewis JL. (2007). Effect of indenter size on elastic modulus of cartilage measured by indentation. *J Biomech Eng.* 129, 767-75.

46. Niada S, Ferreira LMJ, Arrigoni E *et al.* Porcine adipose-derived stem cells from buccal fat pad and subcutaneous adipose tissue for future preclinical studies in oral surgery. *Stem Cell Res Ther.* 4, 148 (2013).
47. Rubina K, Kalinina N, Efimenko A *et al.* Adipose stromal cells stimulate angiogenesis via promoting progenitor cell differentiation, secretion of angiogenic factors, and enhancing vessel maturation. *Tissue Eng Part A.* 15, 2039-50 (2009).
48. Rehman J, Traktuev D, Li J *et al.* Secretion of angiogenic and antiapoptotic factors by human adipose stromal cells. *Circulation.* 109, 1292-8 (2004).
49. Dimarino AM, Caplan AI, Bonfield TL. Mesenchymal Stem Cells in Tissue Repair. *Front Immunol.* 4, 201 (2013).
50. Caplan AI, Dennis JE. Mesenchymal stem cells as trophic mediators. *J Cell Biochem.* 98, 1076-84 (2006).
51. Gonzalez MA, Gonzalez-Rey E, Rico L, Buscher D, Delgado M. Treatment of experimental arthritis by inducing immune tolerance with human adipose-derived mesenchymal stem cells. *Arthritis Rheum.* 60, 1006-19 (2009).
52. Yanez R, Lamana ML, Garcia-Castro J, Colmenero I, Ramirez M, Bueren JA. Adipose tissue-derived mesenchymal stem cells have in vivo immunosuppressive properties applicable for the control of the graft-versus-host disease. *Stem Cells.* 24, 2582-91. (2006).
53. Hare JM, Fishman JE, Gerstenblith G, *et al.* Comparison of allogeneic vs autologous bone marrow-derived mesenchymal stem cells delivered by transendocardial injection in patients with ischemic cardiomyopathy: the POSEIDON randomized trial. *Jama.* 308, 2369-79 (2012).
54. Huang XP, Sun Z, Miyagi Y *et al.* Differentiation of allogeneic mesenchymal stem cells induces immunogenicity and limits their long-term benefits for myocardial repair. *Circulation.* 122, 2419-29 (2010).
55. Sacerdote P, Niada S, Franchi S *et al.* Systemic administration of human adipose-derived stem cells reverts nociceptive hypersensitivity in an experimental model of neuropathy. *Stem Cells Dev.* 22, 1252-63 (2013).
56. Zhu W, Shi XL, Xiao JQ, Gu GX, Ding YT, Ma ZL. Effects of xenogeneic adipose-derived stem cell transplantation on acute-on-chronic liver failure. *Hepatobiliary Pancreat Dis Int.* 12, 60-7 (2013).

#### LEGENDS TO THE FIGURES

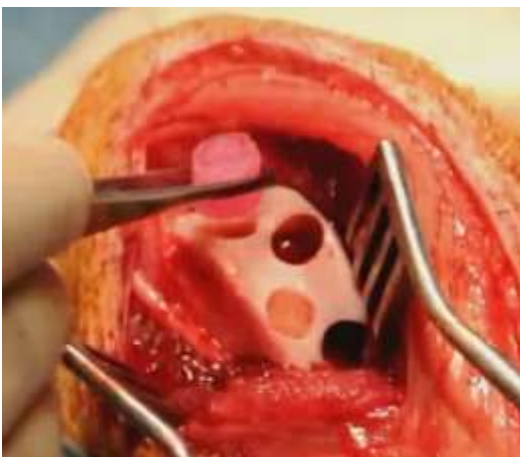


**Figure 1. Surgical technique and constructs implantation.** Osteochondral lesions in the trochlea periphery of the knee joint of a minipig.

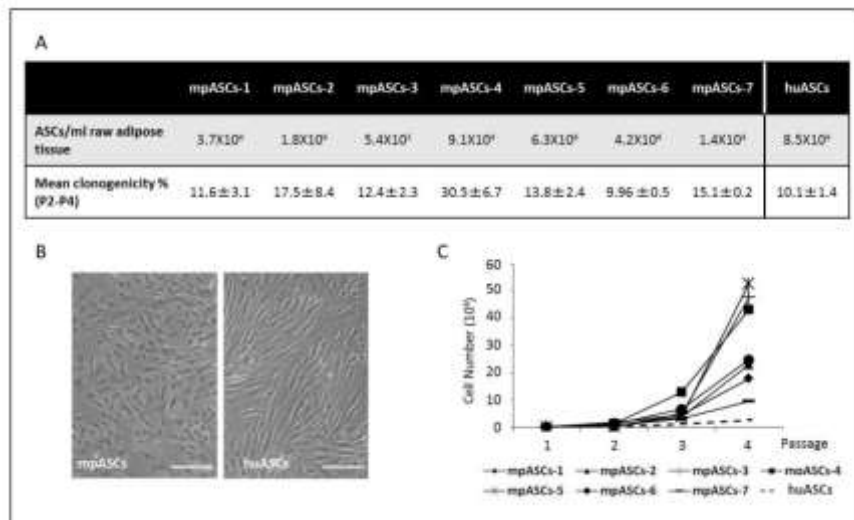


**Figure 2. Isolation and characterization of minipig (mp) and human (hu) ASCs.** Cellular yield and clonogenic ability (expressed as percentage of number of colonies/number of plated cells) of mp- and hu-ASCs (A). Cell morphology at passage 3 (optical microscopy, 40x magnification, scale bar 100µm) (B). Proliferation of ASCs maintained in culture until passage 4 (plating 8x10<sup>4</sup> cells at passage 1) (C).

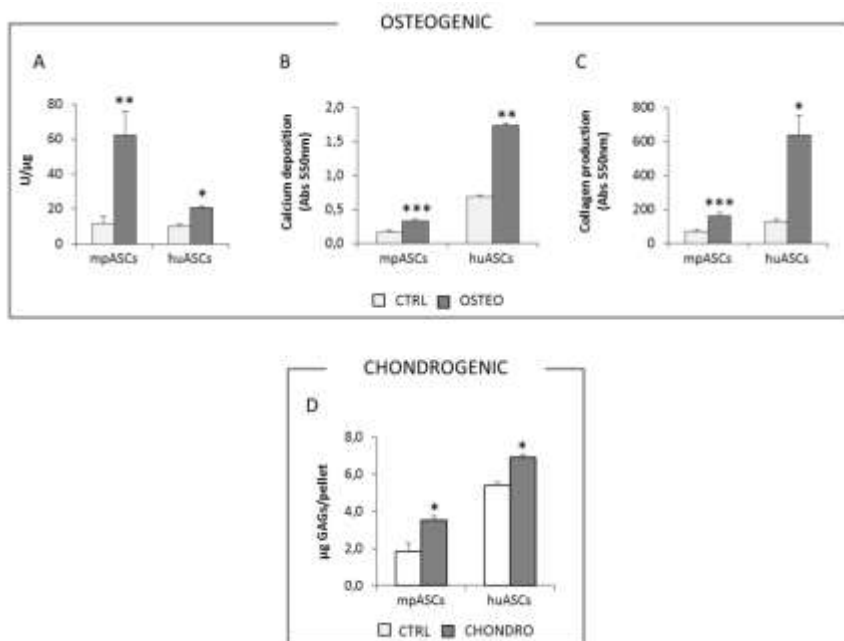


**Figure 3. *In vitro* osteogenic and chondrogenic potential of ASCs.** Alkaline phosphatase activity (A), calcified extracellular matrix (B) and collagen (C) deposition of mp- and hu-ASCs cultured for 14 days in undifferentiated (white bars) and osteogenic (dark bars) medium (n=7). Glycosaminoglycan quantification of undifferentiated (white bars) and chondro-differentiated (dark bars) micromasses expressed as µg of GAGs for each pellet, cultured for 21 days (n=3) (D). Data are expressed as mean ± SEM. Differentiated vs undifferentiated \*p<0.05, \*\*p<0.01, \*\*\*p<0.001. CTRL, undifferentiated cells; OSTEO, osteo-differentiated cells; CHONDR0, chondro-differentiated cells.

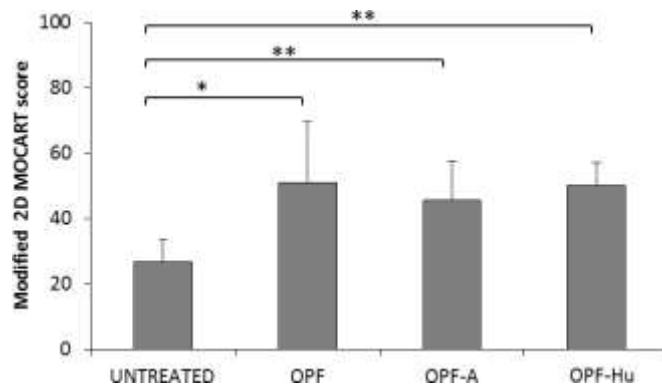


**Figure 4.** Modified 2D MOCART score obtained analysing MR imaging of the ex vivo osteochondral lesions. OPF, unloaded scaffold; OPF-A, OPF seeded with autologous ASCs; OPF-Hu, OPF seeded with human ASCs. \* $p < 0.05$ , \*\* $p < 0.01$ .



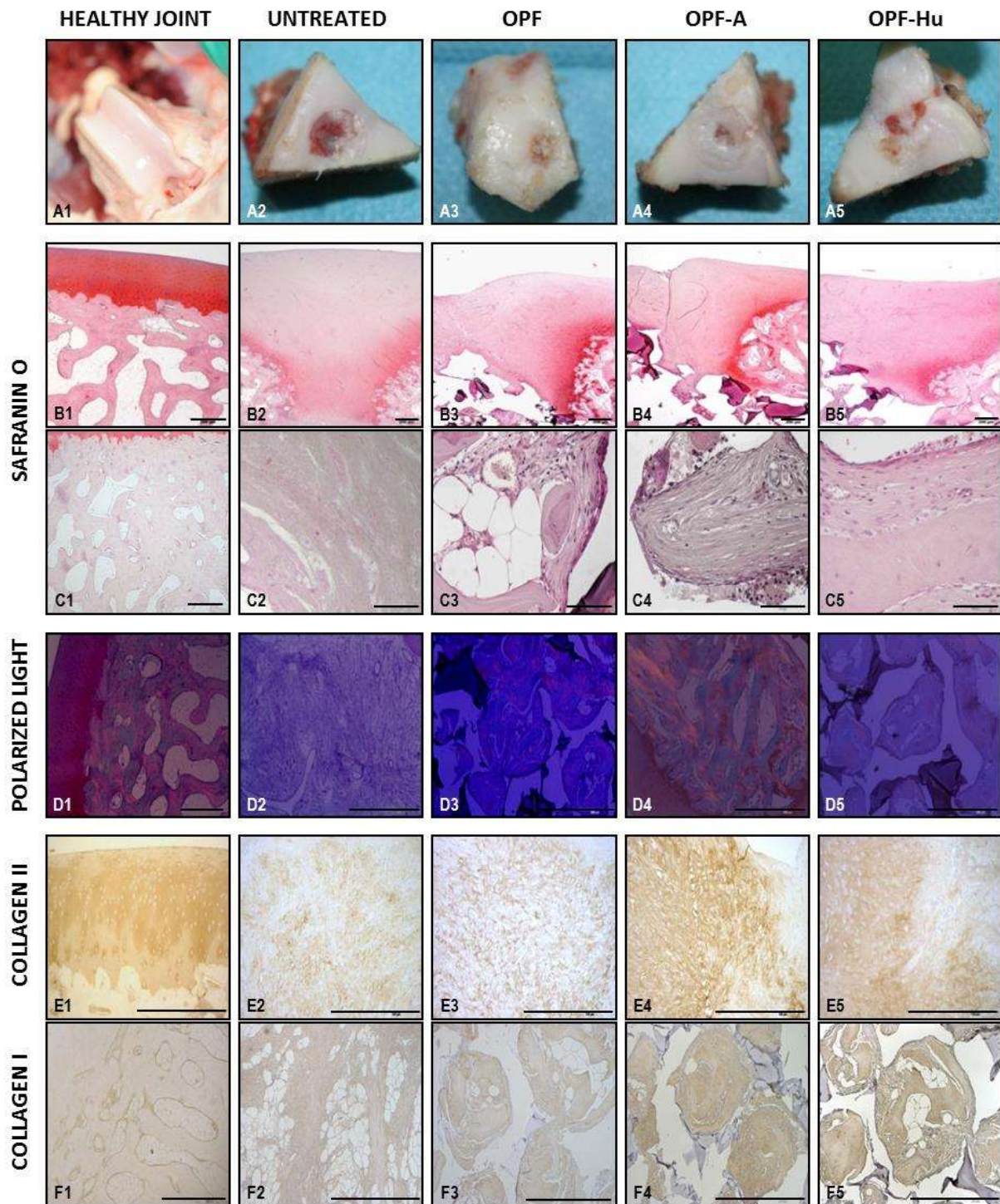


**Figure 5.** Gross appearance (row A) and histological sections (row B-F) of the neo-formed osteochondral tissue formation of the different experimental groups after 6 months from implantation. Sections were stained with Safranin-O (row B – cartilage layer, C – bone layer), analysed by polarized light microscope (row D) and immunostained with type I (row E) and type II collagen (row F). Scale bar: 50µm for C2-C5, 200µm for all the other pictures.

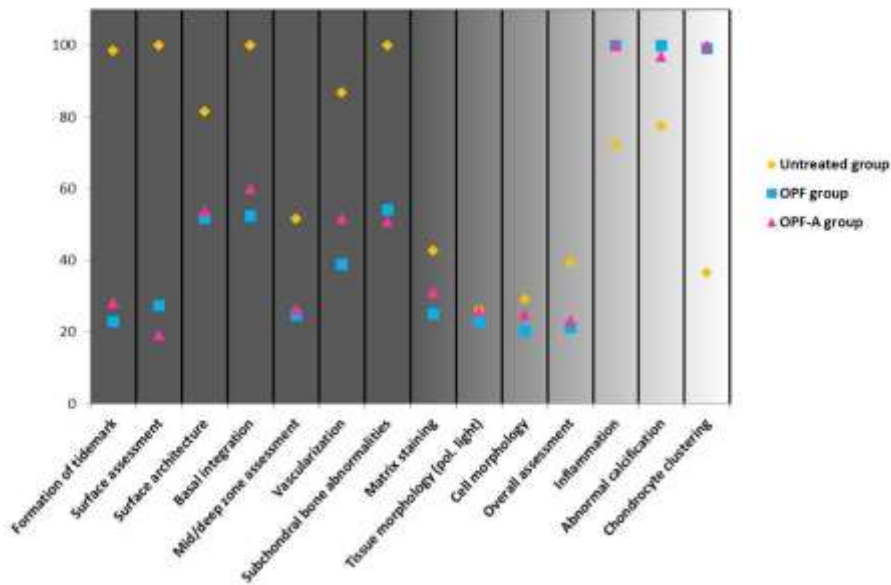


**Figure 6.** ICRS (International Cartilage Repair Society) II score of the neo-formed osteochondral tissue of untreated, OPF and OPF-A groups. All the parameters included in the evaluation forms are depicted in the graph. Three different blind evaluators analysed all the histological sections.

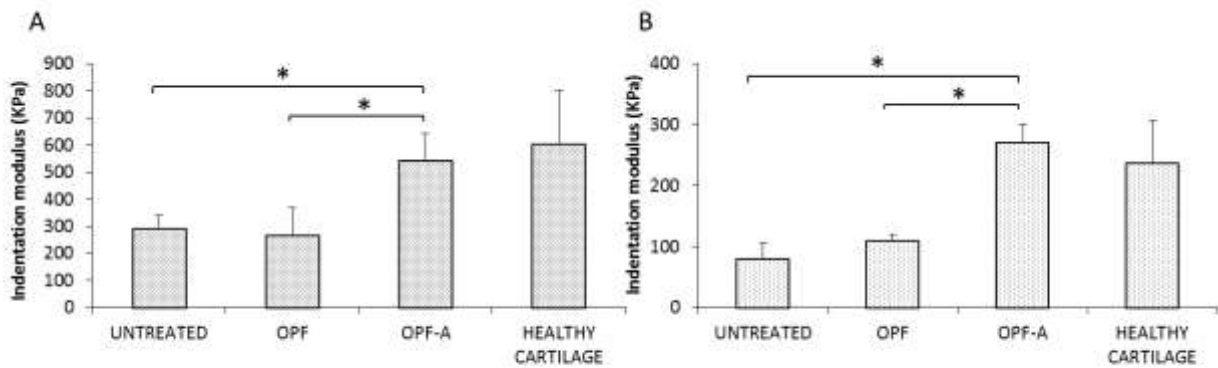


**Figure 7.** Indentation modulus at equilibrium  $M_{e0}$  for untreated samples, OPF, OPF-A and healthy control and for the R<sub>25</sub> (A) and R<sub>400</sub> tip (B). Data are expressed as mean±SD.

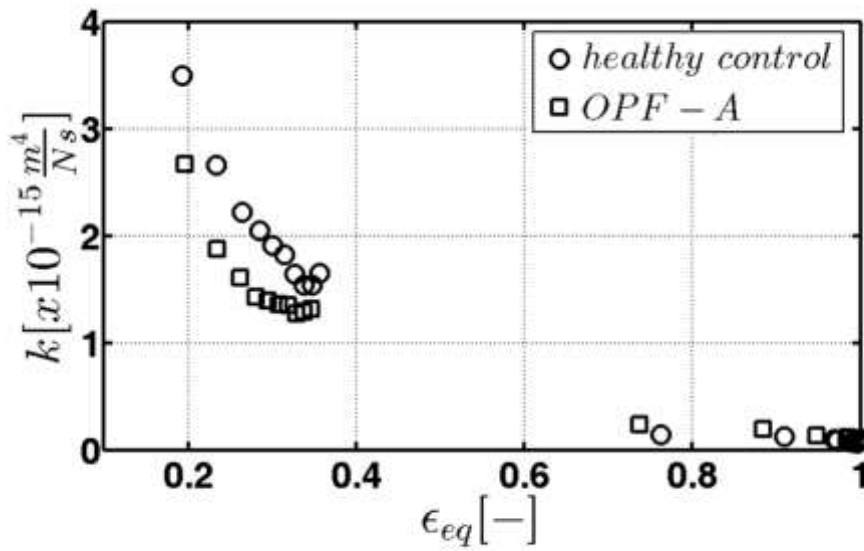


**Figure 8.** Mean permeability values with respect to the equivalent deformation of healthy control and OPF-A.

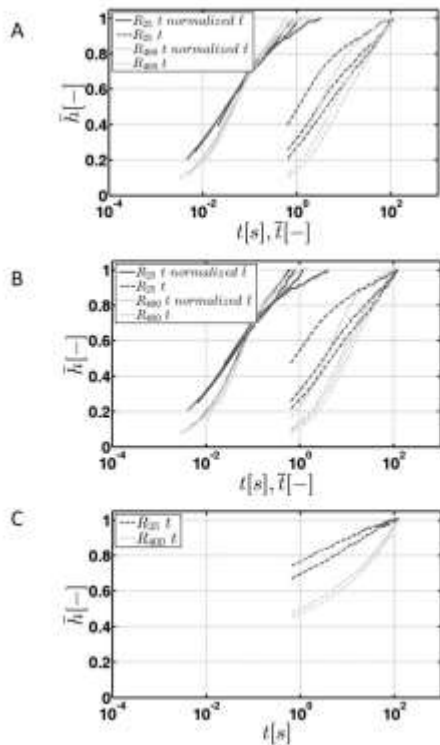


**Figure 9.** Creep curves for the healthy cartilage (A), OPF-A (B) and OPF (C) samples for both R<sub>25</sub> (dark lines) and R<sub>400</sub> (light lines) tips. In (A) and (B), representative curves are shown with respect to natural time  $t$  (dotted lines) and dimensionless time  $\bar{t}$  (continuous lines); in (C) only creep curves with respect to natural time are reported.

Treatment	n
Untreated (UNT)	7
Unseeded scaffold (OPF)	7
OPF + Autologous ASCs (OPF-A)	7
OPF +Allogeneic ASCs (OPF-Allo)	3
OPF + Human ASCs (OPF-Hu)	4

Table 1: Experimental scheme: groups of treatment for the 28 critical osteochondral defects in the minipigs' right knees.

Parameter	Item	Score
<b>Defect fill</b>	<i>Subchondral bone exposed</i>	0
	<i>Incomplete &lt; 50%</i>	5
	<i>Incomplete &gt; 50%</i>	10
	<i>Complete</i>	20
	<i>Hypertrophy</i>	15
<b>Cartilage</b>	<i>Complete</i>	15
	<i>Demarcating border visible</i>	10
	<i>Defect visible &lt; 50%</i>	5
	<i>Defect visible &gt; 50%</i>	0
<b>Surface</b>	<i>Intact</i>	10
	<i>Damaged &lt; 50% of depth</i>	5
	<i>Damaged &gt; 50% of depth</i>	0
<b>Adhesion</b>	<i>Yes</i>	5
	<i>No</i>	0
<b>Structure</b>	<i>Homogeneous</i>	5
	<i>Inhomogeneous or cleft formation</i>	0
<b>Signal intensity</b>	<i>Normal</i>	30
	<i>Nearly normal</i>	10
	<i>Abnormal</i>	0
<b>Subchondral lamina</b>	<i>Intact</i>	5

	<i>Non intact</i>	0
<b>Subchondral bone</b>	<i>Intact</i>	5
	<i>Granulation tissue, cyst, sclerosis</i>	0
<b>Effusion</b>	<i>No</i>	5
	<i>Yes</i>	0

Table 2: 2D MOCART scale developed by Marlovits et al. [30] and modified by Goebel et al. [29]

<b>Histological parameters</b>	<b>Score</b>
Tissue morphology (polarized light)	0: full thickness collagen fibers 100: normal cartilage birefringence
Matrix staining (metachromasia)	0: no staining 100: full metachromasia
Cell morphology	0: no round/oval cells 100: mostly round/oval cells
Chondrocyte clustering (4 or more grouped cells)	0: present 100: absent
Surface architecture	0: delamination or major irregularity 100: smooth surface
Basal integration	0: no integration 100: complete integration
Formation of tidemark	0: no calcification front 100: tidemark
Subchondral bone abnormalities (marrow fibrosis)	0: abnormal 100: normal marrow
Inflammation	0: present 100: absent
Abnormal calcification/ossification	0: present 100: absent
Vascularization (within the repaired tissue)	0: present 100: absent
Surface/superficial assessment	0: total loss or complete destruction 100: resembles intact articular cartilage
Mid/deep zone assessment	0: fibrous tissue 100: normal hyaline cartilage
Overall assessment	0: bad (fibrous tissue) 100: good (hyaline cartilage)

Table 3: ICRS II scoring system (reproduced from Mainil-Varlet et al.[32])

Sample	Tip Radius R [ $\mu\text{m}$ ]	Total Load $F_T$ [mN]	Load steps	Indentation sites
Healthy control	25	0.9	0.1	8
Healthy control	400	1	0.1	6
OPF-A	25	0.7	0.1	3
OPF-A	400	1	0.1	4
OPF	25	1	0.1	4
OPF	400	1	0.1	4
UNT	25	0.3	0.1	5
UNT	400	0.6	0.1	4

Table 4: Maximum load, load step size and total number of indentation sites for each sample type.

